

RADIO EMISSION FROM PULSAR WIND NEBULAE WITHOUT SURROUNDING SUPERNOVA EJECTA: APPLICATION TO FRB 121102

Z. G. DAI^{1,2}, J. S. WANG^{1,2,3}, & Y. W. YU^{4,5}

¹School of Astronomy and Space Science, Nanjing University, Nanjing 210093, China; dzg@nju.edu.cn

²Key Laboratory of Modern Astronomy and Astrophysics (Nanjing University), Ministry of Education, China

³Max-Planck-Institut für Kernphysik, Saupfercheckweg 1, D-69117 Heidelberg, Germany

⁴Institute of Astrophysics, Central China Normal University, Wuhan 430079, China

⁵Key Laboratory of Quark and Lepton Physics (Central China Normal University), Ministry of Education, China

Draft version December 17, 2019

ABSTRACT

In this paper, we propose a new scenario in which a rapidly-rotating strongly magnetized pulsar without any surrounding supernova ejecta produces fast radio bursts (FRBs) repeatedly via some mechanisms, and meanwhile, an ultra-relativistic electron/positron pair wind from the pulsar sweeps up its ambient dense interstellar medium, giving rise to a non-relativistic pulsar wind nebula (PWN). We show that the synchrotron radio emission from such a PWN is bright enough to account for the recently-discovered persistent radio source associated with the repeating FRB 121102 in reasonable ranges of the model parameters. In addition, our PWN scenario is consistent with the non-evolution of the dispersion measure inferred from all the repeating bursts observed in four years.

Subject headings: pulsars: general – radiation mechanisms: non-thermal – radio continuum: general
– stars: neutron

1. INTRODUCTION

Fast radio bursts (FRBs) are millisecond-duration flashes of coherent GHz radio emission of unknown physical origin (Lorimer et al. 2007; Keane et al. 2012; Thornton et al. 2013; Spitler et al. 2014; Champion et al. 2015; Masui et al. 2015; Ravi et al. 2015, 2016; Petroff et al. 2016; Spitler et al. 2016; Chatterjee et al. 2017). Most of them arise from high Galactic latitudes, but their inferred dispersion measures, $DM \sim 300 - 1600 \text{ pc cm}^{-3}$, are much larger than expected for propagation through the cold plasma of the Galaxy and its halo, strongly suggesting that they are at cosmological distances (for a review on observations and models see Katz 2016a).

Only one repeating case, FRB 121102, was first detected to occur on 2 November 2012 (Spitler et al. 2014). Surprisingly, 10, 6, and 13 additional bright bursts from the direction of this FRB were reported to appear only in three different times, respectively (Spitler et al. 2016; Scholz et al. 2016; Chatterjee et al. 2017; Marcote et al. 2017), appearing to indicate a temporally-clustering feature of these repeating bursts. More importantly, the discovery of both persistent radio and optical sources associated with FRB 121102 and the identification of a host dwarf galaxy at a redshift of $z = 0.193$ (Chatterjee et al. 2017; Marcote et al. 2017; Tendulkar et al. 2017) certainly confirm a cosmological origin of this FRB.

These observations rule out the catastrophic event models such as the collapse of supra-massive neutron stars to black holes or the merger of binary compact objects. Four types of radio emission for FRB 121102 have been discussed in detail. First, in the rotationally-powered model (e.g., Connor et al. 2016; Cordes & Wasserman 2016; Lyutikov et al. 2016; Metzger et al. 2017; Kashiyama & Murase 2017), FRBs from a millisecond magnetar are suggested to be a scaled-up version of super-giant pulses from the Crab

pulsar.¹ Second, in the magnetically-powered model (e.g., Popov & Postnov 2010; Kulkarni et al. 2014; Katz 2016b; Metzger et al. 2017; Kashiyama & Murase 2017), FRBs may arise from the unexpected release of magnetic energy (or electrostatic energy see Katz 2017) in the magnetar’s interior, similar to the giant flare model of Galactic magnetars. FRBs might also be driven repeatedly during the accretion of magnetized materials onto a neutron star from its white dwarf companion (Gu et al. 2016). Third, in the gravitationally-powered model (Dai et al. 2016), repeating bursts may originate from a strongly magnetized pulsar encountering an asteroid belt around another star. This model has been shown to explain several previously-observed properties including the duration distribution, repetitive rate, and temporal clustering of the bursts. Fourth, in the kinetically-powered “cosmic-comb” model (Zhang 2017), FRBs may be produced in the magnetosphere of a regular pulsar that is “combed” suddenly and repeatedly by a nearby, strong plasma stream towards the anti-stream direction. No matter which type of energy source is correct, some stringent constraints on the spin period and surface magnetic field strength of the central pulsar have been derived from the recent observations (e.g. Cao et al. 2017).

While the physical origin of FRB 121102 remains controversial, the persistent radio emission source associated with this FRB, which was recently discovered by Chatterjee et al. (2017) and further detected by Marcote et al. (2017), becomes mysterious. Murase et al. (2016) predicted the persistent radio emission from the termination shock produced by the interaction of an ultra-relativistic pulsar wind with the supernova (SN) ejecta,² and very recently,

¹ Kisaka et al. (2017) constrained the parameters of a pulsar powering FRB 121102 based on the giant-pulse emission model from the luminosities and durations of the 30 observed bursts.

² Yang et al. (2016) studied the heating effect of an FRB on its

Kashiyama & Murase (2017) utilized the observed radio data to constrain the parameters of this model. In addition, Metzger et al. (2017) explored the radio emission from the forward shock produced by the interaction between the fast outer layer of SN ejecta with its ambient medium. These works assumed the SN ejecta with a mass $\sim 10M_\odot$. It is so massive SN ejecta that would lead to an observational evolution of DM over the year time scale for a very young age of few decades (Piro 2016; Lyutikov 2017; Metzger et al. 2017). However, the non-detection of DM evolution requires that the SN ejecta should have a much smaller mass. Kashiyama & Murase (2017) suggested one solution to this question, i.e., an ultra-stripped SN with a mass $\lesssim 0.1M_\odot$ is possibly associated with FRB 121102. Piro & Kulkarni (2013) have studied the radio emission from the SN ejecta both that has such a small mass and that is powered by a millisecond magnetar, and found an observational evolution of the radio emission flux over the year time scale. It is not clear whether the persistent radio source associated with FRB 121102 shows a similar evolution.

In this paper, we propose a new scenario for the persistent radio source, in which a rapidly-rotating strongly magnetized pulsar is not surrounded by the SN ejecta. Such a situation may appear if a pulsar has an extremely high kick velocity to leave away far from its birth site (Chatterjee & Cordes 2004; Hobbs et al. 2005) or if a pulsar escapes from its high-mass X-ray binary system during the explosion of its companion star (Bhattacharya & van den Heuvel 1991) or if a pulsar is born and then moves away during the merger of binary neutron stars (Dai et al. 2006; Giacomazzo & Perna 2013; Yu et al. 2015) or the accretion-induced collapse of a white dwarf (Canal & Schatzman 1976; Nomoto & Kondo 1991; Yu et al. 2015). While this pulsar may produce bursts repeatedly through some mechanisms mentioned above, an ultra-relativistic wind from the pulsar is sweeping up its ambient dense interstellar medium, giving rise to a non-relativistic pulsar wind nebula (hereafter PWN) *without surrounding SN ejecta*. We show that our PWN scenario can explain the persistent radio source in reasonable ranges of the model parameters. This paper is organized as follows. In Section 2, we analyze the dynamics of the PWN, and in Section 3, we discuss the properties of synchrotron radio emission from the PWN. In Section 4, we constrain the model parameters and discuss the DM contributed by the PWN and innermost cold wind. Finally, in Section 5, we present our conclusions.

2. DYNAMICS OF A PWN WITHOUT SURROUNDING EJECTA

A highly-magnetized pulsar generates a cold ultra-relativistic wind dominated by electron/positron pairs (maybe including a very small number of baryons) with a luminosity of L_w and a bulk Lorentz factor of Γ_w . This wind sweeps up an ambient dense medium, leading to two shocks: a reverse shock (i.e., a termination shock with a radius of R_t) that propagates into the cold wind and a forward shock that propagates into the ambient medium. Thus, the system has a four-zone structure

ambient self-absorbed synchrotron nebula and found an obvious, detectable hump of the nebula spectrum in several decades near the self-absorption frequency.

consisting of (1) outermost, an unshocked medium with a constant number density of n_0 , (2) next, a forward-shocked medium, (3) a reverse-shocked wind gas (i.e., a PWN without surrounding SN ejecta), and (4) innermost, an unshocked cold wind from the pulsar, where regions 2 and 3 are separated by a contact discontinuity with a radius of R_p . By assuming that a gamma-ray burst is driven by a newborn millisecond magnetar, Dai (2004) studied observational signatures of a post-burst relativistic PWN powered by such a magnetar, and found a plateau in the light curve of an early afterglow due to the reverse shock emission. This feature provides an explanation for the light-curve plateaus of gamma-ray burst afterglows observed by Swift (Yu & Dai 2007). In this paper we investigate the radio emission from a non-relativistic PWN powered by a rapidly-rotating highly-magnetized pulsar.

We first discuss how the system evolves dynamically with time. On one hand, while the heating mechanism of the PWN (region 3) is continuous energy injection from the pulsar, the dominant energy loss of the PWN is work against the forward-shocked medium (region 2), so that the total energy E_3 of the PWN evolves through

$$\frac{dE_3}{dt} = L_w - 4\pi R_p^2 P_2 \frac{dR_p}{dt}, \quad (1)$$

and

$$E_3 = \left(\frac{4\pi}{3} R_p^3\right) \times (3P_3), \quad (2)$$

where t is the dynamically-expanding time of the PWN, P_2 and P_3 are the pressures of regions 2 and 3 respectively, and $P_2 = P_3$ on both sides of the contact discontinuity. Please note that the first factor (volume) on the right side term of equation (2) is taken by assuming $R_t \ll R_p$ and that the second factor is the total energy density of the PWN, $U_3 = 3P_3$.

On the other hand, owing to the work from region 3 and the thin-shell approximation of region 2, the motion of region 2 follows from

$$\frac{d}{dt} \left[M_{sw} \frac{dR_p}{dt} \right] = 4\pi R_p^2 P_3, \quad (3)$$

and

$$M_{sw} = \frac{4\pi}{3} R_p^3 n_0 m_p \quad (4)$$

is the swept-up medium mass, where m_p is the proton mass. Thus, a combination of equations (1) to (4) gives

$$\frac{d}{dt} \left[R_p^2 \frac{d}{dt} \left(M_{sw} \frac{dR_p}{dt} \right) \right] = R_p L_w. \quad (5)$$

Assuming that L_w is constant during the pulsar's spin-down timescale t_{sd} , we obtain a solution to equation (5),

$$R_p = C \left(\frac{L_w t^3}{n_0 m_p} \right)^{1/5} = 1.3 \times 10^{18} \left(\frac{L_{w,41} t_2^3}{n_{0,2}} \right)^{1/5} \text{ cm}, \quad (6)$$

where $C \equiv [125/(224\pi)]^{1/5} = 0.708$, $L_{w,41} = L_w/10^{41} \text{ erg s}^{-1}$, $t_2 = t/10^2 \text{ yr}$, and $n_{0,2} = n_0/10^2 \text{ cm}^{-3}$. This dynamics is similar to that of interstellar wind bubbles (Castor et al. 1975). From equations (2), (3) and

(6), therefore, we can calculate the total energy and energy density of the PWN,

$$E_3 = \frac{28\pi}{25} C^5 L_w t = 2.0 \times 10^{50} L_{w,41} t_2 \text{ erg}, \quad (7)$$

and

$$U_3 = \frac{E_3}{(4\pi/3)R_p^3} = 2.3 \times 10^{-5} L_{w,41}^{2/5} n_{0,2}^{3/5} t_2^{-4/5} \text{ erg cm}^{-3}. \quad (8)$$

According to Gaensler & Slane (2006), we obtain the radius of the termination shock

$$R_t \simeq \left(\frac{L_w}{4\pi c P_3} \right)^{1/2} = 1.9 \times 10^{17} L_{w,41}^{3/10} n_{0,2}^{-3/10} t_2^{2/5} \text{ cm}, \quad (9)$$

where c is the speed of light. It can be seen from equations (6) and (9) that the assumption $R_t \ll R_p$ is indeed valid if typical values of the model parameters are taken.

3. SYNCHROTRON RADIO RADIATION FROM THE PWN

We next discuss synchrotron radio radiation from the PWN. Electrons (and positrons) in the cold pulsar wind (region 4) are accelerated to ultra-relativistic energies by the termination shock at R_t and fill the PWN out to R_p . We assume that their power-law spectrum behind the shock front is $dn_e/d\gamma_e = K\gamma_e^{-p}$ in units of electrons cm^{-3} . Their synchrotron emission spectrum depends on three break frequencies. We consider the hard electron spectrum (i.e., $1 < p < 2$) in this paper.

The first break frequency is the synchrotron cooling frequency at which an electron with the cooling Lorentz factor γ_c loses its energy in a dynamical time t . From Sari et al. (1998), we get the cooling Lorentz factor

$$\gamma_c = \frac{6\pi m_e c}{\sigma_T B 2t} = 4.3 \times 10^2 \epsilon_B^{-1} L_{w,41}^{-2/5} n_{0,2}^{-3/5} t_2^{-1/5}, \quad (10)$$

where m_e is the electron mass, σ_T is the Thomson cross-section, and $B = (8\pi\epsilon_B U_3)^{1/2} = 2.4 \times 10^{-2} \epsilon_B^{1/2} L_{w,41}^{1/5} n_{0,2}^{3/10} t_2^{-2/5}$ G is the magnetic field strength in the PWN under the assumption that the magnetic energy density behind the shock is a fraction ϵ_B of the total energy density. Thus, the synchrotron cooling frequency is calculated by

$$\nu_c = \gamma_c^2 \frac{q_e B}{2\pi m_e c} = 1.2 \times 10^{10} \epsilon_B^{-3/2} L_{w,41}^{-3/5} n_{0,2}^{-9/10} t_2^{-4/5} \text{ Hz}, \quad (11)$$

where q_e is the electron charge.

Owing to this cooling effect, the electron spectrum behind the termination shock becomes (Sari et al. 1998)

$$\frac{dn_e}{d\gamma_e} = \begin{cases} K\gamma_e^{-p}, & \gamma_{\min} \leq \gamma_e < \gamma_c, \\ K\gamma_c\gamma_e^{-(p+1)}, & \gamma_c \leq \gamma_e \leq \gamma_{\max}, \end{cases} \quad (12)$$

where γ_{\min} and γ_{\max} are the minimum and maximum Lorentz factors of the shock-accelerated electrons, respectively. Here we only discuss the slow-cooling regime to account for the spectrum of the persistent radio source associated with FRB 121102. In the following calculations, we fix $p = 1.4$ (Chatterjee et al. 2017).

We further assume that the electron energy density behind the shock is a fraction ϵ_e of the total energy density,

$$U_e = \epsilon_e U_3 = \int_{\gamma_{\min}}^{\gamma_{\max}} \left(\frac{dn_e}{d\gamma_e} \right) (\gamma_e m_e c^2) d\gamma_e. \quad (13)$$

Please note that $\epsilon_e + \epsilon_B = 1$ in our PWN scenario. Inserting equation (12) into equation (13), we find

$$K = \frac{(2-p)(p-1)\epsilon_e U_3}{m_e c^2 \gamma_c^{2-p}} = 0.18 \epsilon_e \epsilon_B^{3/5} L_{w,41}^{16/25} n_{0,2}^{24/25} t_2^{-17/25} \text{ cm}^{-3}. \quad (14)$$

The second break frequency is the typical synchrotron frequency which an electron with γ_{\min} radiates,

$$\nu_m = \gamma_{\min}^2 \frac{q_e B}{2\pi m_e c} = 6.7 \times 10^4 \epsilon_B^{1/2} \gamma_{\min}^2 L_{w,41}^{1/5} n_{0,2}^{3/10} t_2^{-2/5} \text{ Hz}. \quad (15)$$

The third break frequency is the synchrotron self-absorption frequency (Wu et al. 2003),

$$\nu_a = \left(\frac{c_2 q_e K R_p}{B} \right)^{2/(p+4)} \frac{q_e B}{2\pi m_e c} = 6.8 \times 10^8 \epsilon_e^{10/27} \epsilon_B^{29/54} \times L_{w,41}^{59/135} n_{0,2}^{127/270} t_2^{-38/135} \text{ Hz} \quad (16)$$

for $\nu_m < \nu_a < \nu_c$, where the coefficient c_2 depends on p (see Appendix A of Wu et al. 2003).

The peak flux density at a luminosity distance of D_L from the source is calculated by (Sari et al. 1998)

$$F_{\nu, \max} = \frac{N_e}{4\pi D_L^2} \frac{m_e c^2 \sigma_T}{3q_e} B = 3.1 \times 10^4 \epsilon_e \epsilon_B^{11/10} \gamma_{\min}^{-(p-1)} \times L_{w,41}^{36/25} n_{0,2}^{33/50} t_2^{18/25} \mu\text{Jy}, \quad (17)$$

where $N_e = 4\pi R_p^3 K / [3(p-1)\gamma_{\min}^{p-1}]$ is the total electron number of the PWN. The synchrotron emission flux density at any frequency ν is given by (Mészáros & Rees 1997; Sari et al. 1998)

$$F_\nu = \begin{cases} F_{\nu, \max} (\nu_a / \nu_m)^{-(p-1)/2} (\nu / \nu_a)^{5/2}, & \nu < \nu_a, \\ F_{\nu, \max} (\nu / \nu_m)^{-(p-1)/2}, & \nu_a < \nu < \nu_c, \\ F_{\nu, \max} (\nu_c / \nu_m)^{-(p-1)/2} (\nu / \nu_c)^{-p/2}, & \nu \geq \nu_c. \end{cases} \quad (18)$$

After inserting equations (15) and (17) into (18), *it is interesting to note that F_ν is independent of γ_{\min} for any value of p* . Thus, we can compare our PWN scenario with the observations on the persistent radio source associated with FRB 121102 to constrain four remaining parameters (L_w , n_0 , ϵ_B , and t) in the next section.

4. CONSTRAINTS ON THE MODEL PARAMETERS

The Very Large Array-observed spectrum (F_ν) of the persistent radio source associated with FRB 121102 (see Extended Data Figure 2 of Chatterjee et al. 2017) indicates the spectral index $\alpha \sim -0.2$ for $\nu \lesssim 10$ GHz and $\alpha \sim -0.8$ for $\nu \gtrsim 10$ GHz. Compared with equation (18), this emission spectrum is consistent with the hard electron spectrum $p \sim 1.4$, and thus the observations require that (i) $\nu_c \simeq 10$ GHz, (ii) $F_{10 \text{ GHz}} \simeq 200 \mu\text{Jy}$, and (iii) $\nu_a \lesssim 1.4$ GHz, in our PWN scenario.

The other requirements are as follows: (iv) The size of the PWN should be smaller than the observed upper limit on the size of the persistent radio source

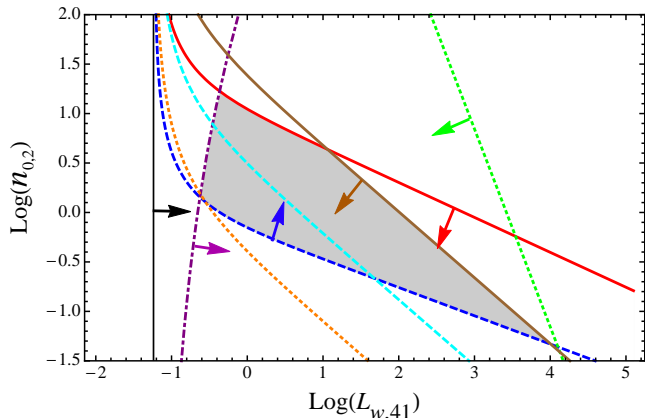


FIG. 1.— Constraints on $L_{w,41}$ and $n_{0,2}$ from requirements (iii, red solid line), (iv, blue dashed line), (v, green dotted line), and (vi, purple dot-dashed line), and (vii, brown solid line), as shown in the text. The cyan dashed line and orange dotted line are plotted based on equation (20) for $t = 40$ and 400 yr, respectively. The black solid line is corresponding to $\epsilon_B > 0$. The shaded region includes the permitted values of $L_{w,41}$ and $n_{0,2}$.

(Marcote et al. 2017), $R_p \lesssim 0.7$ pc. (v) The radius of the termination shock, R_t , must be much smaller than the radius of the contact discontinuity, R_p , in order that our PWN scenario is self-consistent. (vi) The DM contributed from the shocked medium should be smaller than the estimated host-galaxy DM (Tendulkar et al. 2017; Cao et al. 2017; Yang et al. 2017), $\text{DM}_{\text{ISM}} = n_0 R_p \lesssim \text{DM}_{\text{host}} \sim 100 \text{ pc cm}^{-3}$. (vii) The age of the PWN should be larger than the total observation period of time, $t \gtrsim 4$ yr.

According to the seven requirements listed above, we can constrain $L_{w,41}$ and $n_{0,2}$. Figure 1 presents these constraints on the $L_{w,41}$ and $n_{0,2}$ plane. On one hand, from requirements (i) and (ii), we obtain

$$\epsilon_B \simeq 1 - 0.06 L_{w,41}^{-1}, \quad (19)$$

where $L_{w,41} > 0.06$ must be satisfied (as shown in Figure 1) so that $\epsilon_B > 0$, and

$$t_2 \simeq 1.3 L_{w,41}^{-3/4} n_{0,2}^{-9/8} \epsilon_B^{-15/8}. \quad (20)$$

On the other hand, by considering requirements (iii)-(vii), we obtain the constraints on $L_{w,41}$ and $n_{0,2}$ from requirements (iii, red solid line), (iv, blue dashed line), (vi, purple dot-dashed line), and (vii, brown solid line). The shaded region in Figure 1 includes the permitted values of $L_{w,41}$ and $n_{0,2}$. In addition, once $L_{w,41}$ and $n_{0,2}$ are given, ϵ_B and t can be calculated from equations (19) and (20).

Now let's further discuss constraints on the period and surface dipole magnetic field strength of the pulsar for given $L_{w,41}$ and t_2 . We assume that P_* is the initial period of the pulsar when it starts to drive the PWN, I is its moment of inertia, B_* is the pulsar's surface dipole magnetic field strength, and R_* is the stellar radius. The pulsar's spin-down luminosity and timescale due to magnetic dipole radiation are estimated by

$$L_{\text{sd}} = 3.8 \times 10^{43} B_{*,12}^2 P_{*,-3}^{-4} R_{*,6}^6 \text{ erg s}^{-1}, \quad (21)$$

and

$$t_{\text{sd}} = 16 B_{*,12}^{-2} P_{*,-3}^2 I_{45} R_{*,6}^{-6} \text{ yr}, \quad (22)$$

respectively, where $B_{*,12} = B_*/10^{12}$ G, $P_{*,-3} = P_*/1$ ms, $I_{45} = I/10^{45}$ g cm², and $R_{*,6} = R_*/10^6$ cm. If $t \lesssim t_{\text{sd}}$ and $L_w = L_{\text{sd}} \simeq \text{constant}$ are required to guarantee the validity of equation (6), then we find

$$P_{*,-3} \lesssim 7.8 L_{w,41}^{-1/2} t_2^{-1/2} I_{45}^{1/2}, \quad (23)$$

and

$$B_{*,12} \lesssim 3.2 L_{w,41}^{-1/2} t_2^{-1} I_{45} R_{*,6}^{-3}. \quad (24)$$

This constraint on B_* for $L_w \gtrsim 10^{41}$ erg s⁻¹ is not inconsistent with the limits based on the rotationally-powered model (see equation 7 in Lyutikov 2017) and the gravitationally-powered model (see equations 9 and 16 in Dai et al. 2016) of FRBs. Of course, there is no limit on B_* in the magnetically-powered model, provided that the average magnetic field strength in the pulsar's interior is high enough (e.g. Metzger et al. 2017).

In the above calculations, we have not taken into account any contribution of the pulsar wind regions (including the PWN and innermost cold wind) to the DM of FRB 121102. In fact, a large number of electrons and positrons are required to exist in the PWN to produce the radio emission. The density of these leptons can be estimated to be $n_e = (2m_p/m_e)n_0/\Gamma_w$ by considering the pressure balance at the contact discontinuity, $P_3 \equiv (1/3) \times 4\Gamma_w n_e m_e c^2 = P_2 \equiv (2/3) \times 4n_0 m_p c^2$. As a result, the DM contributed by the PWN is about $\text{DM}_{\text{PWN}} = n_e R_p = 15 L_{w,41}^{1/5} n_{0,2}^{4/5} t_2^{3/5} \Gamma_{w,4}^{-1} \text{ pc cm}^{-3}$, which is basically consistent with the upper limit of $\text{DM}_{\text{PWN,max}} \lesssim 100 \text{ pc cm}^{-3}$, where $\Gamma_{w,4} = \Gamma_w/10^4$. However, as pointed out by Cao et al. (2017), this large number of leptons should come from a much smaller radius ($\lesssim R_t$) and even from the light cylinder of the pulsar, where the lepton density and the Lorentz factor are much higher and thus a higher DM could be caused. In particular, from Yu (2014) and Cao et al. (2017), a stringent constraint on the spin period can be found by requiring the DM of the total free wind to be smaller than the upper limit of $\text{DM}_{w,\text{max}}$, that is, $P_{*,-3} \gtrsim 6.0 \mu_{\pm,lc}^{2/3} L_{w,41}^{2/3} R_{*,6}^{-4} \text{DM}_{w,\text{max},2}^{-1}$, where $\mu_{\pm,lc}$ is the multiplicity that represents the ratio of the wind lepton flux at the light cylinder to the Goldreich-Julian flux ($\dot{N}_{\text{GJ}} = 2.8 \times 10^{34} L_{w,41}^{1/2} R_6^{-3} \text{ s}^{-1}$), and $\text{DM}_{w,\text{max},2} = \text{DM}_{w,\text{max}}/10^2 \text{ pc cm}^{-3}$. This constraint for $L_w \gtrsim 10^{41}$ erg s⁻¹ is basically in agreement with equation (23), if the DM contribution of the pulsar wind can be comparable to that of the host galaxy and if the lepton density at the light cylinder does not significantly deviate from the Goldreich-Julian density.

5. CONCLUSIONS

In this paper we have proposed a new scenario for the recently-discovered persistent radio source associated with FRB 121102, in which a rapidly-rotating strongly magnetized pulsar has not been surrounded by the SN ejecta. This pulsar may produce bursts repeatedly through the rotationally-powered or magnetically-powered or gravitationally-powered mechanisms listed in the introductory section, and meanwhile an ultra-relativistic electron/positron pair wind from the pulsar interacts with its ambient dense interstellar medium, leading to a non-relativistic PWN without surrounding

SN ejecta. We studied the dynamics and synchrotron radio emission from such a PWN in detail. By fitting the observed radio spectrum, we constrained the model parameters and found that all the parameters are in their reasonable ranges. Therefore, our PWN scenario can provide an explanation for the persistent radio source associated with FRB 121102. Furthermore, from requirement (vi) and discussions in Section 4, the time derivative of the DM contributed from the source, $dDM_{\text{src}}/dt \lesssim DM_{\text{src,max}}/t \sim 1DM_{\text{src,max},2}t_2^{-1} \text{ pc cm}^{-3} \text{ yr}^{-1}$, is unde-

tectable and thus consistent with the non-evolution of the DM inferred from all the repeating bursts observed in four years (where $DM_{\text{src,max}}$ is the maximum DM from the source, including the contributions of the innermost free wind, PWN, and shocked medium).

We thank Bing Zhang for helpful comments and suggestions. This work was supported by the National Basic Research Program (“973” Program) of China (grant No. 2014CB845800) and the National Natural Science Foundation of China (grant Nos. 11473008 and 11573014).

REFERENCES

- Bhattacharya, D., & van den Heuvel, E. P. J. 1991, *Phys. Rep.*, 203, 1
- Canal, R., & Schatzman, E. 1976, *ã*, 46, 229
- Cao, X. F., Yu, Y. W., & Dai, Z. G. 2017, arXiv:1701.05482
- Castor, J., McCray, R., & Weaver, R. 1975, *ApJ*, 200, L107
- Champion, D. J., Petroff, E., Kramer, M. et al. 2015, *MNRAS*, 460, L30
- Chatterjee, S., & Cordes, J.M. 2004, *ApJ*, 600, L51
- Chatterjee, S., Law, C. J., Wharton, R. S. et al. 2017, *Nature*, 541, 58
- Connor, L., Sievers, J., & Pen, U.-L. 2016, *MNRAS*, 458, L19
- Cordes, J. M., & Wasserman, I. 2016, *MNRAS*, 457, 232
- Dai, Z. G. 2004, *ApJ*, 606, 1000
- Dai, Z. G., Wang, X. Y., Wu, X. F., & Zhang, B. 2006, *Science*, 311, 1127
- Dai, Z. G., Wang, J. S., Wu, X. F., & Huang, Y. F. 2016, *ApJ*, 829, 27
- Gaensler, B. M., & Slane, P. O. 2006, *ARA&A*, 44, 17
- Giacomazzo, B., & Perna, R. 2013, *ApJ*, 771, L26
- Gu, W. M., Dong, Y. Z., Liu, T., Ma, R., & Wang, J. 2016, *ApJ*, 823, L28
- Hobbs, G., Lorimer, D.R., Lyne, A.G., & Kramer, M. 2005, *MNRAS*, 360, 974
- Kashiyama, K., & Murase, K. 2017, arXiv:1701.04815
- Katz, J. I. 2016a, *Modern Physics Letters A*, 31, 1630013
- Katz, J. I. 2016b, *ApJ*, 826, 226
- Katz, J. I. 2017, arXiv:1702.02161
- Keane, E. F., Stappers, B. W., Kramer, M., & Lyne, A. G. 2012, *MNRAS*, 425, L71
- Kisaka, S., Enoto, T., & Shibata, S. 2017, arXiv:1702.02922
- Kulkarni, S. R., Ofek, E. O., Neill, J. D., Zheng, Z., & Juric, M. 2014, *ApJ*, 797, 70
- Lorimer, D. R., Bailes, M., McLaughlin, M. A., Narkevic, D. J., & Crawford, F. 2007, *Science*, 318, 777
- Lyutikov, M. 2017, arXiv:1701.02003
- Lyutikov, M., Burzawa, L., & Popov, S. B. 2016, *MNRAS*, 462, 94
- Marcote, B., Paragi, Z., Hessels, J. W. T. et al. 2017, *ApJ*, 834, L8
- Masui, K., Lin, H.-H., Sievers, J. et al. 2015, *Nature*, 528, 523
- Mészáros, P., & Rees, M. J. 1997, *ApJ*, 476, 232
- Metzger, B. D., Berger, E., & Margalit, B. 2017, arXiv:1701.02370
- Murase, K., Kashiyama, K., & Mészáros, P. 2016, *MNRAS*, 461, 1498
- Nomoto, K., & Kondo, Y. 1991, *ApJ*, 367, L19
- Piro, A. L. 2016, *ApJ*, 824, L32
- Piro, A. L., & Kulkarni, S. R. 2013, *ApJ*, 762, L17
- Petroff, E., Barr, E. D., Jameson, A. et al. 2016, *PASA*, 33, e045
- Popov, S. B., & Postnov, K. A. 2010, *Evolution of Cosmic Objects through their Physical Activity* (edited by Harutyunian, H. A., Mickaelian, A. M., & Terzian, Y.), p. 129-132
- Ravi, V., Shannon, R. M., & Jameson, A. 2015, *ApJ*, 799, L5
- Ravi, V., Shannon, R. M., Bailes, M. et al. 2016, *Science*, 354, 1249
- Sari, R., Piran, T., & Narayan, R. 1998, *ApJ*, 497, L17
- Scholz, P., Spitler, L. G., Hessels, J. W. T. et al. 2016, *ApJ*, 833, 177
- Tendulkar, S. P., Bassa, C. G., Cordes, J. M. et al. 2017, *ApJ*, 834, L7
- Spitler, L. G., Cordes, J. M., Hessels, J. W. T. et al. 2014, *ApJ*, 790, 101
- Spitler, L. G., Scholz, P., Hessels, J. W. T. et al. 2016, *Nature*, 531, 202
- Thornton, D., Stappers, B., Bailes, M. et al. 2013, *Science*, 341, 53
- Wu, X. F., Dai, Z. G., Huang, Y. F., & Lu, T. 2003, *MNRAS*, 342, 1131
- Yang, Y. P., Zhang, B., & Dai, Z. G. 2016, *ApJ*, 819, L12
- Yang, Y. P., Luo, R., Li, Z., & Zhang, B. 2017, arXiv:1702.06465
- Yu, Y. W. 2014, *ApJ*, 796, 93
- Yu, Y. W., & Dai, Z. G. 2007, *A&A*, 470, 119
- Yu, Y. W., Li, S. Z., Dai, Z. G. 2015, *ApJ*, 806, L6
- Zhang, B. 2017, arXiv:1701.04094